Evaluation of Elasto-Plastic Interfacial Fracture Parameters in Solder-Copper Bimaterial Using Moiré Interferometry

H. Krishnamoorthy
Graduate Student.

H. V. Tippur
Assoc. Professor.
Mem. ASME.
htippur@eng.auburn.edu

Failure Characterization & Optical Techniques Lab,
Department of Mechanical Engineering,
Auburn University, 202 Ross Hall,
Auburn, AL 36849-5341

An experimental investigation dealing with failure characterization of 63/37 solder-copper interfaces is presented. The method of moiré interferometry is used for mapping elasto-plastic deformations in bimaterials subjected to predominantly tensile loading. A method for quantifying the fracture parameter—the J-integral—using full-field measurement of crack opening displacements has been developed. A linear relationship between crack tip opening displacements (CTOD) and the J-integral is demonstrated. The crack growth resistance curve and hence crack initiation toughness J_c value for the bimaterial is obtained. Full-field optical information has also suggested the possibility of using a simpler method for the J-integral estimation using a single strain gage for fracture testing of interfaces with large mismatch in this geometry.

1 Introduction

The Sn-Pb based solders are routinely used to attach the surface mounted devices to the printed circuit boards. Solder not only provides electrical but also mechanical connection between the electronic component and the printed circuit board. In these situations, copper is a common lead material in contact with the solder, and often stress induced failures are seen at these joints due to mechanical overload, thermal shock, fatigue, thermal expansion mismatch, thermal gradients, geometry effects, etc. The formation of intermetallics at the interface embrittle the interface and make it susceptible to cracking.

Failure characterization of solder-copper joints is complex owing to the nonlinear, rate-dependent characteristics of solder (Busso, et al. 1992; Skipor, et al. 1996). Fracture parameter measurements in 63/37 solder at different temperatures have been reported by Logsdon et al. (1990). At the moment, information on failure characterization of the solder-copper joints, particularly from the interfacial fracture mechanics point of view, is rather limited. Yamada (1989) has reported critical values of 60/40 solder-beryllium copper joints by testing double cantilever beams subjected to monotonic loading. Creep-fatigue interactions in surface-mounted solder joints has been studied by Enke et al. (1989). They have presented data for monotonic loading, fatigue, and creep-fatigue loading for 60/40 tin-lead solder lap joints at room temperature. Mode-I fracture toughness testing of eutectic solder-copper joints has been reported by Pratt et al. (1994). They have measured the fracture toughness of solder-copper joints using ASTM standard methods similar to homogeneous material testing. Skipor et al. (1995) have studied the effect of mechanical constraint on the flow and fracture of 63Sn-37Pb eutectic solder alloy.

At the moment, very little experimental work on elasto-plastic interfacial crack tip fields and validation of the proposed models is reported. The primary objective of the present investigation is to map full-field deformations and develop techniques for characterizing solder-copper interfacial fracture. This paper is limited to techniques to accomplish the same objective with predominantly tensile loading conditions. First, mapping crack opening displacements using full-field optical method of moiré interferometry is undertaken. Using a single displacement component field, various fracture parameters, namely, the J-integral, crack tip opening displacement, mode-mixity, and crack initiation toughness are obtained for 63/37 solder-copper interfaces at room temperature. The measurements are also examined in light of prevailing knowledge on elasto-plastic fracture mechanics. Lastly, the full-field optical measurements have also revealed the possibility of a simpler method of evaluating J-integral using strain gages in three-point-bend loading configuration.

2 Experimental Technique and Optical Setup

The optical setup for mapping displacements using moiré method is shown in Fig. 1. It essentially consists of an existing Mach-Zehnder interferometer (Sinha, et al., 1997) modified for performing moiré interferometry. The optical components include a He-Ne laser, a collimator, beam splitters (BS1 and BS2), mirrors (M1 and M2), and an imaging camera. The collimated laser beam entering the interferometer is split into two paths 1 and 2, as shown by the beam splitter BS1 and the mirrors. The laser beams emerging from the beam splitter BS2 are made to intersect at an angle by the optical elements to create a standing wave in space. When a specimen with gratings of the same pitch are introduced in this space, moiré fringes are formed on its surface. The interference patterns from the experiments are captured by a camera. The imaging axis of the camera makes a small angle θ (15–18°) with the x_3-axis in the $x_2 - x_3$ plane, and is used in determining the fringe location (y-coordinate). The angle between the laser beams (50 mm in diameter) is adjusted to obtain a standing wave of the desired pitch, p,

$$p = \frac{\lambda}{2 \sin \frac{\beta}{2}}, \tag{1}$$

where λ is the wave length of the laser light, and β is the angle between the two intersecting light beams. Under no-load conditions, the angle β is adjusted such that the pitch of the virtual gratings coincide with that of the sample gratings and a

Contributed by the Electrical and Electronic Packaging Division for publication in the JOURNAL OF ELECTRONIC PACKAGING. Manuscript received by the EEPD February 25, 1997; revision received March 24, 1998. Associate Technical Editor: D. T. Read.

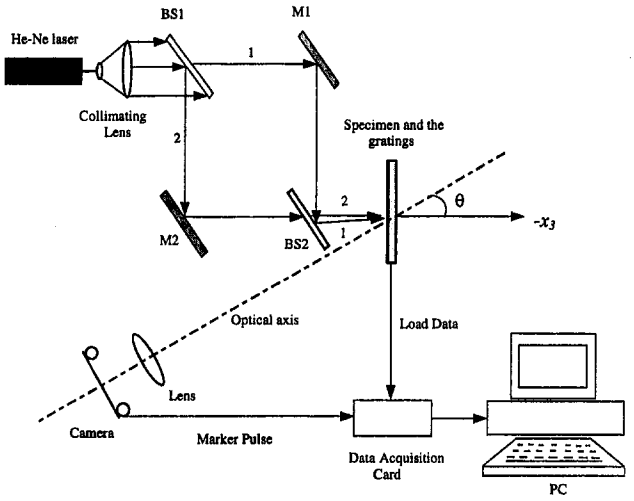

Fig. 1 Schematic of the optical setup for moiré interferometry

uniform light field interference is formed. When the sample deforms, the frequency and the orientation of the sample gratings vary spatially. The interference between the sample and the virtual gratings result in the formation of moiré fringes representing displacement contours. The component of the displacement is determined by the principal direction of the sample gratings. In this paper, only the crack opening displacements (u_2-displacement components) have been mapped. The displacement, the fringe order, and the pitch of the gratings are related by,

$$u_2 = Np, \tag{2}$$

where N denote fringe orders ($=0, \pm1, \pm2, \pm3, \ldots$). The experiments reported in this work were conducted with grating pitch of 8 μm. This choice was based on the extensive elasto-plastic deformations anticipated in the solder side of solder-copper bimaterials.

3 Calibration Experiments: Elastic Interfacial Crack

3.1 Sample Preparation. Before proceeding to study the solder-copper interfaces, where plasticity effects dominate the crack tip region, a brittle interface made of polymer-metal joint was investigated, and the technique based on optical measurements was tested. In these experiments, PMMA-aluminum bimaterial samples ($150 \times 25 \times 5$ mm) were made by bonding the aluminum and PMMA (polymethylmethacrylate) halves using methylmethacrylate (MMA) monomer and a polymerizing agent. The aluminum half was sandblasted to enhance the bond strength. The MMA monomer and a polymerizing agent were mixed, and a thin coating of the mixture was applied to the edge of the aluminum half to be bonded. A thin, pliable Teflon tape ($\sim$50 μm thick) was introduced between the two halves to produce an edge crack ($a/W = 0.25$, W being the width of the sample). The sample was subjected to a constant pressure, and cured at room temperature. Subsequently, one of the faces of the bimaterial sample was prepared using #600 and #1000 fixed abrasives, and a thin aluminum film (about a micron thick) was deposited on this face of the sample in the interfacial region using e-beam evaporation. This provided uniform and enhanced reflectivity to the bimaterial surface. Subsequently, the face was coated with a positive photoresist, and Ronchi gratings (square wave profile gratings) of pitch 8 μm were printed using optical lithography with lines parallel to the interface.

3.2 Optical Mapping. The sample was placed in the loading frame, and a uniform light field optical interference was obtained under no-load conditions. The bimaterial beams were subjected to monotonic, quasi-static, three point bending using a displacement controlled loading device at a rate of 3×10^{-5} m/s. The crack opening displacement field (u_2) and the load data were acquired from no-load condition to crack initiation and growth using a motorized camera and a data acquisition system. The camera recorded the displacement fringes at a rate of one frame per second. A marker pulse, sent by the camera each time the shutter opened, was also acquired by the data acquisition system and was used to get a correspondence between the load record and the interference patterns. The three-point-bend configuration and a typical u_2-displacement field near the interfacial crack are shown in Fig. 2. Here, the fringe patterns correspond to the case of a quasi-statically propagating crack along the interface. The crack length a at this instance was approximately 8 mm.

3.3 J-integral Estimation Using Crack Opening Displacement Measurements. A few investigations reported in the literature have used measured displacement and strain data for estimating the J-integrals in homogeneous fracture specimens. Read (1981) has presented a method to experimentally evaluate the J-integral in ductile materials using strain gages, crack mouth opening displacement gages, and linear variable differential transducers (LVDT). A method of using both crack opening (u_2) and crack sliding (u_1) displacements has been proposed by Kang and Kobayashi (1988) to measure the J-integral in homogeneous ductile samples in uniaxial tensile loading conditions.

Here, we propose using only crack opening displacement data to estimate the J-integral,

$$J = \int_\Gamma \left(W dx_2 - \sigma_{ij} n_j \frac{\partial u_i}{\partial x_1} ds \right), \tag{3}$$

in bimaterial beams loaded in three-point-bending configuration by considering a closed contour Γ around the crack tip. In the above, $W = (1/2)\sigma_{ij}\varepsilon_{ij}$, is the strain energy density, u_i, σ_{ij}, ε_{ij} are the displacement, stress, and strain components, respectively, ds is an elemental length, and n_j are the components of the unit vector normal to the closed contour Γ. The above equation can be expanded as,

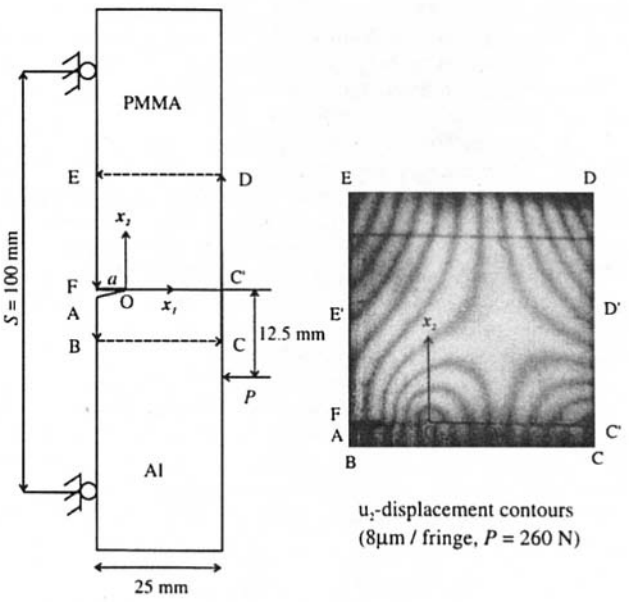

Fig. 2 Three point bending configuration for PMMA-aluminum bimaterial sample and a typical u_2 displacement field

$$J = \int_\Gamma W dx_2 - \int_\Gamma (\sigma_{11} n_1 + \sigma_{12} n_2) \frac{\partial u_1}{\partial x_1} ds - \int_\Gamma (\sigma_{12} n_1 + \sigma_{22} n_2) \frac{\partial u_2}{\partial x_1} ds. \quad (4)$$

Considering the closed rectangular path OABCDEFO, as shown in Fig. 2, along the boundaries of the sample around the crack tip,

$$J_\Gamma = J_{OA} + J_{AB} + J_{BC} + J_{CD} + J_{DE} + J_{EF} + J_{FO}. \quad (5)$$

The following observations and assumptions can be made for different segments of this path.

Paths OA and FO. The crack flanks represented by OA and FO are stress free ($\sigma_{22} = \sigma_{12} = 0$, $n_1 = 0$, $n_2 = 1$), and, hence, do not contribute to the J-integral. Therefore, $J_{OA} = J_{FO} = 0$.

Paths AB and CC′. The surface represented by the paths AB and CC′ are traction free, i.e., $\sigma_{11} = \sigma_{12} = 0$. Also, $n_1 = \mp 1$, $n_2 = 0$. It can be seen from Fig. 2 that the u_2-displacement contours are parallel to the x_2-axis and are equally spaced in the aluminum side (simple rotation) of the bimaterial (which implies that the u_1-displacement contours are also equally spaced and parallel to the x_1-axis). Hence, all the in-plane strain components, $\varepsilon_{11} = (\partial u_1/\partial x_1) \approx 0$, $\varepsilon_{22} = (\partial u_2/\partial x_2) \approx 0$, and $2\varepsilon_{12} = (\partial u_1/\partial x_2) + (\partial u_2/\partial x_1) \approx 0$ (with cross derivatives being equal and of opposite sign). Thus, the second and the third integrals are zero in Eq. (4). The first integral is also negligible because the strain component ε_{22} is approximately zero. Hence, J_{AB}, $J_{CC'}$ are negligible.

Path BC. In this case, points B and C have the same x_2-coordinate; hence, the first integral vanishes. Also, $n_1 = 0$, $n_2 = -1$, and $\partial u_1/\partial x_1 \approx 0$; hence, the second integral is approximately zero. The third integral is neglected since all the strain components are approximately zero. Thus, the overall contribution from this segment (J_{BC}) is negligible.

Paths C′D and EF. These paths are on the PMMA side of the bimaterial. From the full-field data, bunching of the u_2-displacement fringes along the path C′D near the interface suggests significant deformations on the PMMA side. The normal strain in the x_2-direction (ε_{22}) along C′D does contribute to the first integral. However, the second and the third integrals are zero (see arguments made for path CC′). Hence, the main contribution to the J-integral comes from the elastic strain energy stored in PMMA. That is,

$$J_{CC'} = \int_{CC'} \frac{E}{2} \varepsilon_{22}^2 dx_2, \quad J_{EF} = \int_{EF} \frac{E}{2} \varepsilon_{22}^2 dx_2. \quad (6)$$

The strain ε_{22} can be measured by differentiating the u_2-displacements in the x_2-direction ($\varepsilon_{22} \approx p(\Delta N/\Delta x_2)$).

Path DE. Along this path, again, $n_1 = 0$, $n_2 = -1$, and $(\partial u_1/\partial x_1) \approx 0$ (as u_2-fringes are nearly parallel to the x_2-axis). Hence, the contribution of the first and the second integrals are negligibly small. The only term remaining is the third integral,

$$J_{DE} = \int_{DE} \sigma_{22} \frac{\partial u_2}{\partial x_1} dx_1. \quad (7)$$

Again, σ_{22} can be expressed in terms of strain components that are negligibly small (u_2-fringes being nearly parallel to the x_2-axis). Hence, σ_{22} is approximately zero along this path. Therefore, $J_{DE} \approx 0$.

It should also be emphasized that the contribution to the J-integral away from the interface in the region D′D and EE′ essentially cancel with each other because flexural deformations dominate far away from the crack tip and the two integration paths are in the opposing directions. The bulk of the contribution to the J-integral comes from the region C′D′ (see Fig. 2). The J-integral estimated using the experimental data for the case shown in Fig. 2 is, $J \approx 320 \pm 20$ N/m. This value agrees well with the $J \approx 305 \pm 20$ N/m obtained from the full-field analysis of the interference patterns (Krishnamoorthy and Tippur, 1998). An independent finite element analysis was also carried out for this geometry, and the J-integral was computed by considering a line integral around the crack tip. The value obtained from numerical simulation was 330 N/m, and is again in agreement with the measured data. The J-integral estimated using the moiré data for a sequence of fringe patterns (not shown here) from no-load condition to failure is shown in Fig. 3(a). The solid symbols represent estimated data, and the dotted line is the best fit for the data. The J-integral and applied load follow a parabolic relationship as one would expect. Using the measured J-integral values, the magnitude of the stress intensity factor, $|Ka^{ie}| = \sqrt{J(E + E_A)/2EE_A}$, is calculated ($E$ and E_A being the Young's moduli of PMMA and aluminum, respectively). A plot of the stress intensity factor and the applied load is shown in Fig. 3(b), and a linear relationship between the two is evident.

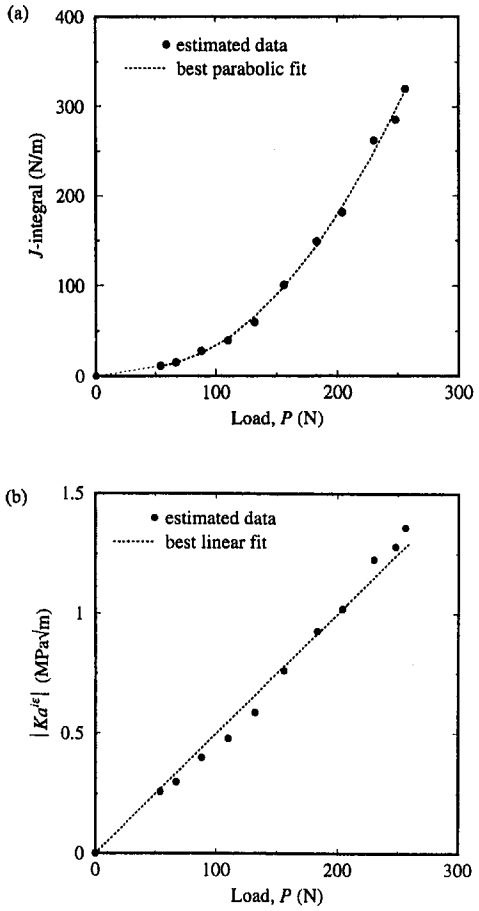

Fig. 3 Variation of (*a*) *J*-integral and (*b*) magnitude of complex stress intensity factor with applied load for PMMA-aluminum bimaterial

4 Interfacial Failure of Solder-Copper Interfaces

Next, the method of evaluating J-integral from optically measured displacement data is extended to situations when crack tip deformations are elasto-plastic in nature.

4.1 Sample Preparation. Solder-copper bimaterial samples (150 × 12 × 5 mm) with edge cracks ($a/W = 0.33$, W being the width of the sample) were prepared by joining solder and copper bars (75 × 12.5 × 6 mm) machined from commer-

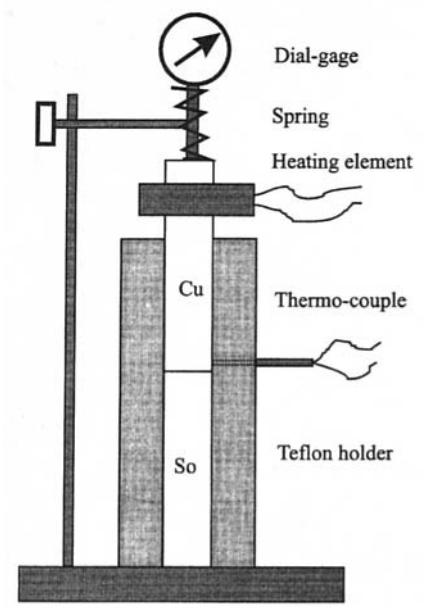

Fig. 4 Schematic of the setup for solder-copper bimaterial preparation

cially available strips. A Teflon fixture was specially designed and fabricated for preparing the bimaterials. The joining of solder and copper bars were done with the help of the Teflon holder, a mica heater, a spring-loaded dial gage and a thermocouple. Figure 4 shows the schematic of the setup. An edge crack was obtained by applying RMA soldering flux to the edges of the bars where bonding was needed, and it was allowed to stay until the flux became tacky. The disbond thus obtained acts as a crack. The solder bar was placed inside the Teflon fixture and the copper bar was placed over it. The spring-loaded dial gage that was placed on top of the copper bar applied a small pressure to improve contact necessary for good heat transfer. The dial gage was used to monitor any movement due to melting of solder at approximately 360°F. The top portion of the copper bar was heated using a mica foil heater. The temperature near the interface was monitored using a thermocouple. The heating was stopped as soon as a movement in the dial gage was observed, indicating the occurrence of melting in the interfacial region. The sample was then cooled to room temperature in air and subsequently finished to the final dimensions. The surface of the sample was prepared using #600 and #1000 fixed abrasives. The interfacial region was then coated with a positive photoresist and Ronchi gratings of pitch 8 μm were printed with the lines parallel to interface using optical lithography.

4.2 Experimental Results. The sample was placed in the loading frame and a uniform light field interference was obtained under no load conditions by adjusting the interferometer. The samples were subjected to monotonic quasi-static three point bending using a displacement-controlled loading device at a rate of 3×10^{-5} m/s. The crack opening displacement field (u_2), and the load data were acquired for approximately 60 seconds from no-load condition to crack initiation and growth by a motorized camera and a data acquisition system. The camera recorded the displacement fringes at a rate of 30 frames per minute. The marker pulse, sent by the camera each time the shutter opens, was also acquired by the data acquisition system and was used to get a correspondence between the load data and the interference patterns. Three-point-bending experiments were conducted with support distances (S) of 75 and 100 mm. The loading configuration and typical patterns of u_2-displacement field near the interfacial crack are shown in Fig. 5. A few selected fringe patterns from a sequence of u_2-displacement fringes from no-load condition to crack initiation and growth are shown in Fig. 6.

4.3 J-integral Estimation. The normal strain ε_{22} near the crack tip on the solder side of the bimaterial can be estimated from the optical data. The strains were greater than the yield strain ($\varepsilon_0 \approx 0.001$ for solder) even during early stages of the loading history, and plasticity was seen to spread quickly on the solder side of the bimaterial. Hence, equations describing elastic interfacial crack tip displacements are no longer valid in these experiments. Explicit closed-form field equations describing interfacial crack tip deformations for such elasto-plastic conditions are currently unavailable (Sharma and Aravas, 1991) for performing full-field analysis of the optical data as in elastic counterparts (Krishnamoorthy and Tippur, 1998).

The J-integral can be estimated by taking a closed contour around the crack tip using the displacement data in the same way discussed earlier in subsection 3.3. Many of the observations and assumptions used in the PMMA-aluminum case hold good for solder-copper bimaterials as well. The fringes parallel to the x_2-axis seen on the copper side of the bimaterial imply a simple rotation of the copper half. Using the same arguments made for the elastic bimaterial in section 3, $J_{AB} = J_{BC} = J_{CC'} = J_{DE} = 0$ and $J_\Gamma = J_{C'D} + J_{EF}$. The plastic dissipation in solder along the path-C′D is the main contributor to the J-integral and is evident from the bunching of the fringes seen in the region C′D′ (see Fig. 5). The strain energy density was calculated on the solder side along C′D and EF using

$$W = \frac{m}{m+1}\sigma_{22}\varepsilon_{22}, \tag{8}$$

where m is the strain hardening index of solder. The stress-strain data for 63/37 solder have been recently reported by Skipor et al. (1996) for various strain rates. The ones corresponding to the current experiments ($\dot{\varepsilon} \approx 10^{-4}$/s) are shown in Fig. 7. The data were fitted using strain hardening material description of the form

$$\frac{\varepsilon}{\varepsilon_0} \approx \alpha\left(\frac{\sigma}{\sigma_0}\right)^m \tag{9}$$

in the nonlinear region of the stress-strain curve beyond the

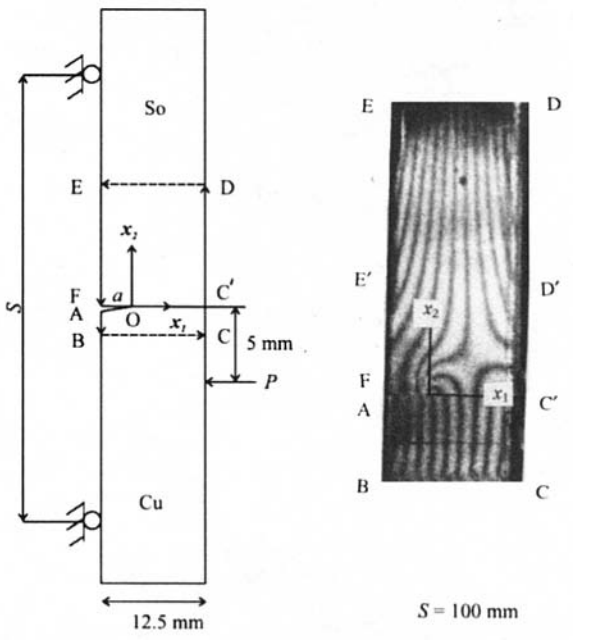

Fig. 5 Solder-copper bimaterial loading configuration and a typical u_2 displacement field

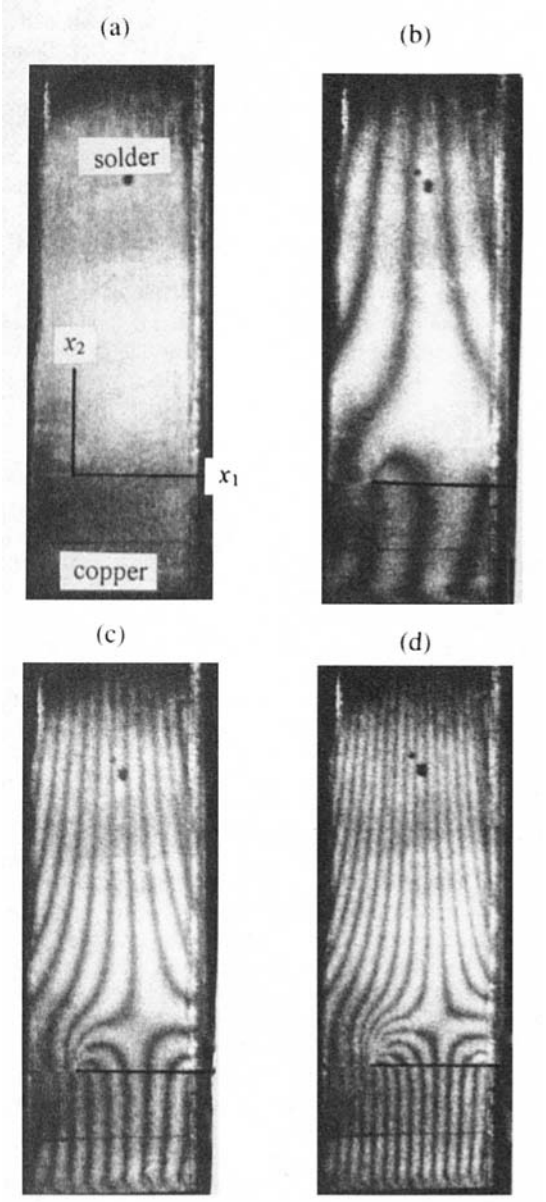

Fig. 6 Selected interferograms from a sequence of moiré fringes for solder-copper experiments (specimen # sc/8/S100): (*a*) P = 0; (*b*) P = 210 N; (*c*) P = 264 N; and (*d*) P = 273 N.

yield stress σ_0. In the above, ε_0 is the yield strain for solder. The values of the parameters m and α were obtained from the fit and were used for the strain energy density calculation when the strains were plastic. The additional details of the material properties for 63/37 solder and copper are provided in Table 1. The stress, σ_{22}, can be related to the strain, ε_{22}, in uniaxial situations as

$$\sigma_{22} = \sigma_0 \left(\frac{\varepsilon_{22}}{\alpha \varepsilon_0} \right)^{1/m} \tag{10}$$

The J-integral was calculated using the material properties listed in Table 1 and the optical measurements. The normal strain, ε_{22}, was calculated by numerically differentiating the u_2-displacements with respect to the x_2-coordinate ($\varepsilon_{22} \approx p\Delta N/\Delta x_2$). The J-integral values were estimated for different load levels, beginning from the frame where sufficient fringes were available for the estimation process until when the resolution of the fringes became difficult due to high fringe densities (resulting from large deformations). The estimated values of the

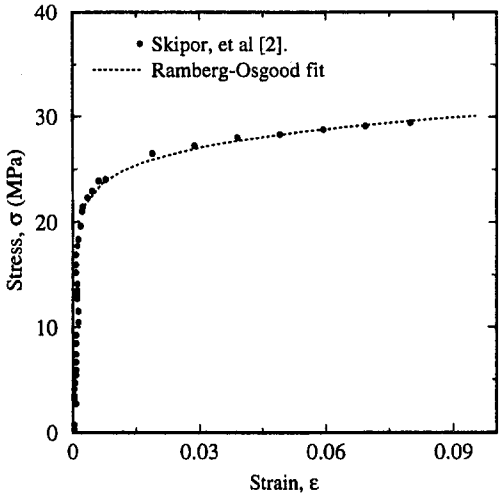

Fig. 7 Stress-strain data for 63/37 solder

Table 1 Material properties of 63/37 solder and copper

Material	E (GPa)	ν	σ_0 (MPa)	m	α
63/37 solder	20	0.4	20	11	1
Copper	124	0.33	70	—	—

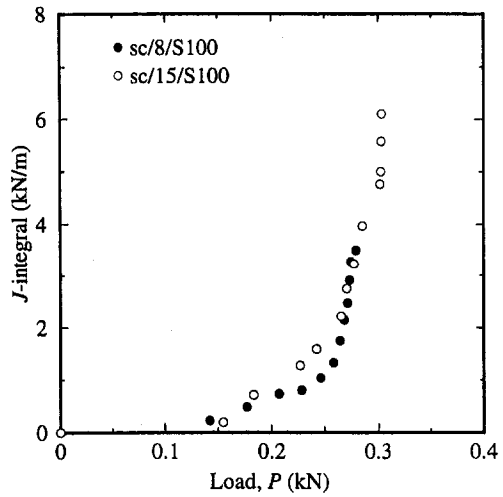

Fig. 8 Variation of J-integral with applied load. Legends indicate specimen number.

J-integral thus obtained are plotted as a function of the applied load (P) in Fig. 8. The variation of J-P curve is similar to the ones seen in ductile fracture counterparts in homogeneous materials. The value of the J-integral grows rapidly at a saturation load of approximately 0.3 kN.

The u_2-displacement data can also be used to measure the crack tip opening displacements (CTOD) commonly used in failure characterization. In this investigation, since optical mapping involved only crack opening displacements, crack blunting could not be investigated due to the lack of u_1-displacement data near the crack tip. Hence, an ad hoc procedure of estimating CTOD was adopted. This was done simply by counting the total number of fringes surrounding the crack AOF at a distance of r = 0.5 mm behind the crack tip, O, multiplied by the grating pitch. A plot of CTOD versus load is shown in Fig. 9(a). The variation of CTOD is similar to that of J-integral, suggesting simple relationship between the J-integral and CTOD. In Fig.

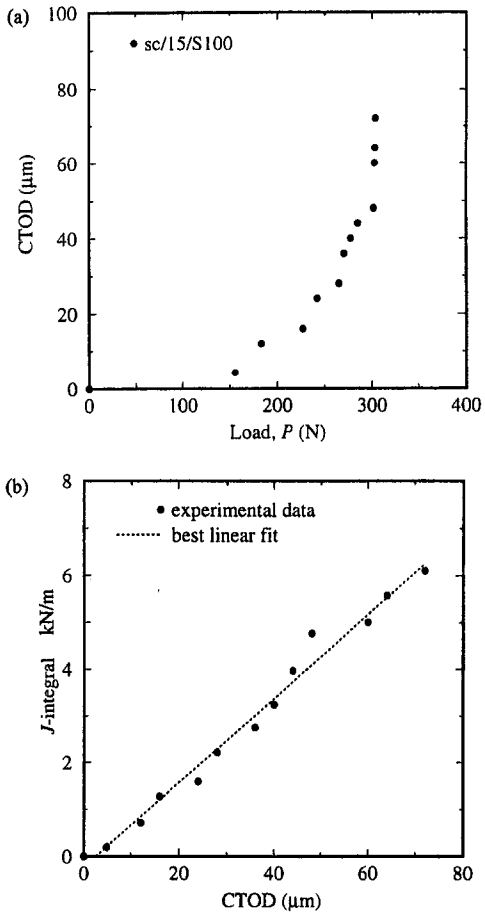

Fig. 9 (*a*) Plot of crack tip opening displacement against applied load (legend indicates specimen number); (*b*) linear relationship between the *J*-integral and crack tip opening displacement.

9(*b*), a plot of CTOD versus *J*-integral shows an approximately linear relationship between the two quantities (Shih, 1981). This observation is similar to the homogeneous counterparts demonstrated in ductile materials. Also recently for bimaterials, Shih and Asaro (1989) have demonstrated

$$\text{CTOD} = d(\alpha\varepsilon_0, m, \xi)\frac{J}{\sigma_o} \tag{11}$$

through computations. In Eq. (11), ξ is the plastic mode-mixity (to be discussed later), and d is a proportionality factor. In this case, the value of d from measurements (prior to crack initiation) is in the range of 0.3–0.4. The reported value, however, is 0.57. The fact that an ad hoc definition for measuring the CTOD used in this work instead of the standard 45 deg offset method with blunted cracks is potentially responsible for this difference.

The quantity of significance from an interfacial failure point of view is the value of the *J*-integral at crack initiation. To measure this parameter, the estimated values of J were plotted against the crack growth (Δa) (Fig. 10) to obtain crack growth resistance curve. The value of Δa was measured from the interferograms. The location of the crack tip was inferred from the discontinuity in the fringes across the interface due to crack growth. The critical value of *J*-integral (J_C) is identified as the value at which the crack initiation occurs. From the plot, J_C can be estimated and is in the range of 1950–2100 N/m for solder-copper joints for the predominantly tensile loading conditions used in this study. In this context, it should be noted that for 60/40 solder-beryllium copper interface a J_C value of approximately 1200 N/m is reported by Yamada (1989). The critical value of stress intensity factor, K_{cr} can be obtained using effective young's modulus E^* ($=2E_1E_2/(E_1 + E_2)$; E_1 and E_2 being Young's modulus of solder and copper, respectively) for the bimaterial. If one were to assume small-scale yielding and plane stress to be valid in this case, then K_{cr} ($J_C = |K_{cr}^2/E^*|$,) can be calculated and is in the range of 8.5–8.8 MPa$\sqrt{\text{m}}$. It should be emphasized that small-scale yielding might be a rather poor assumption in this case. This value seems to agree reasonably well with the one equal to 8.0 MPa$\sqrt{\text{m}}$ reported by Pratt et al. (1994) for the same interface using copper-solder copper sandwiches.

Interfacial failure is inherently mixed mode in nature. Therefore, mode mixity (or phase angle) was estimated based on the concepts developed by Shih (1991):

$$\xi = \left\{\psi + \varepsilon \ln\left(\frac{JE^*}{\sigma_0^2 L}\right)\right\}\Bigg|_{L=a}, \tag{12}$$

where ξ is the plastic phase angle, ψ is the elastic phase angle, σ_0 is the yield stress of the softer of the two materials, ε is the oscillation index ($\sim$0.064), and L is the characteristic length (assumed to be the initial crack length). The plastic mode mixities were calculated, and are plotted against the applied load, P, in Fig. 11. The elastic phase angle, ψ, necessary for this, was obtained from O'Dowd et al. (1992) as 6.5 deg for three-point-bending configuration. The mode mixity at crack initiation thus calculated is approximately 21 deg. It should be noted that ξ is defined in the context of small-scale yielding, and, hence, the plastic mixity values reported here may be more appropriate in the early stages of the loading history. Also, after crack initiation, the mode mixity would depend on the crack length. However, for this geometry and material combination, the changes in the phase angle over the range $a/W = 0.33$ to 0.5 result in an elastic phase angle change (ψ) of less than one degree. Hence, mode mixity changes due to crack extension are assumed to be negligible compared to the ones due to plasticity. For the sake of completeness, a plot of *J*-integral versus total mode mixity is shown in Fig. 11(*b*). In here, the post crack initiation values (J_C) are noted by the broken line.

5 *J*-Estimation Using Strain Gage Measurements

It can be seen from the full-field data (Fig. 5) that the bulk of the deformations occur primarily in the solder half of the bimaterial. For a integration path used in this work, the contribution essentially comes from a select region near the interface. The fringes near the interface in solder along the edge C′D′

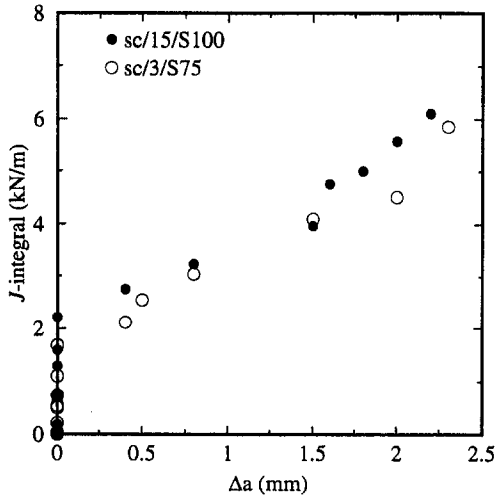

Fig. 10 Crack growth resistance curve for 63/37 solder-copper bimaterial (legends indicate specimen number)

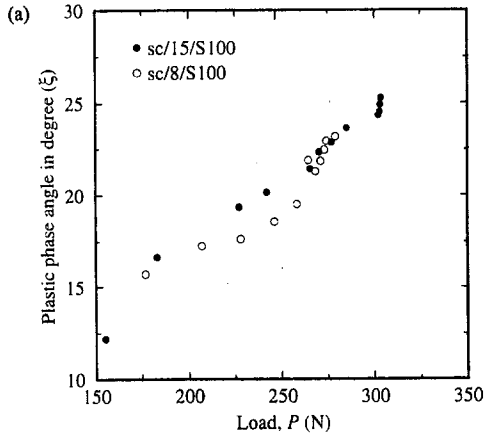

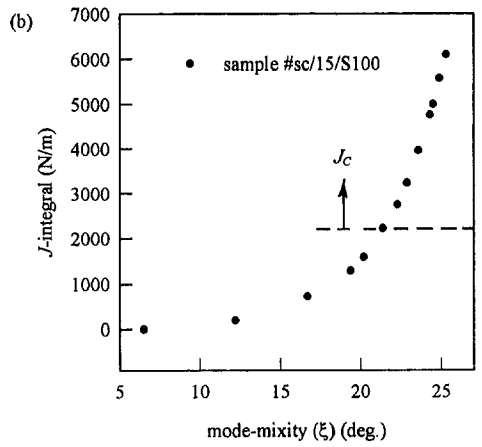

Fig. 11 Variation of (*a*) plastic mode-mixity with applied load; (*b*) Measured *J*-integral with mode-mixity for solder-copper bimaterial (legends indicate specimen number).

opposing the crack tip mainly contribute to the *J*-integral. Further, the fringe spacing along C′D′ are approximately equally spaced suggesting that the strain ε_{22} is relatively constant over this length. The contribution to the *J*-integral from D′D and EE′ are relatively small and approximately cancel with each other due to the opposing sense of the integration paths. Thus, the bulk of the contribution to the *J*-integral comes from the region C′D′ as the contribution from E′F is negligibly small. From the interference patterns, the size of the region C′D′ was estimated and is about 6 mm in the current sample geometry. Strain gages of gage length 6 mm were mounted in the region C′D′ and E′F. The strain data were acquired simultaneously by the data acquisition system during the experiment and were subsequently used to estimate the *J*-integral. The strain data obtained from the two strain gages are shown in Fig. 12. It is seen from the figure that the strain in the region E′F is negligible when compared to the ones from the region C′D′ suggesting that a single strain gage data is sufficient for estimating the J_C. The *J*-integral was estimated using

$$J \approx \frac{m}{m+1}\sigma_0\left(\frac{\varepsilon_{22}}{\alpha\varepsilon_0}\right)^{1/m}\varepsilon_{22}\Delta l, \qquad (13)$$

where ε_{22} is the average strain in the region C′D′ over the gage length Δl. Here, $m = 1$ was used when strains were elastic while $m = 11$ was used when plastic with α being unity. The values so calculated are plotted against the applied load in Fig. 13. Superposed on this data are the *J*-integral estimates obtained from the u_2-displacement measurement using moiré interferometry. A good agreement between the two suggests that this is a potentially attractive technique for estimating J_C for solder-copper interfaces in three-point-bending tests.

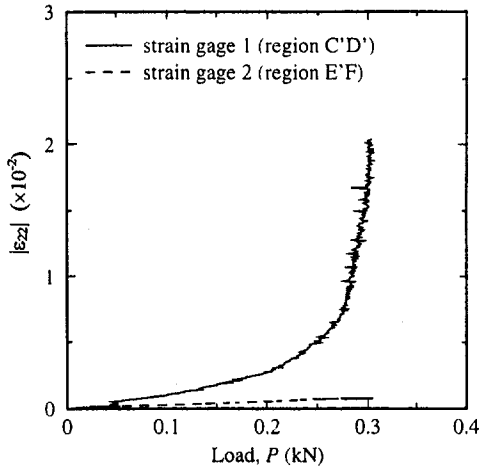

Fig. 12 Acquired strain (magnitude) data against applied load

Conclusions

Failure characterization of 63/37 solder-copper bimaterial is undertaken, and techniques for interfacial fracture parameter extraction are reported. The method of moiré interferometry is used to optically map elasto-plastic crack opening displacements in three-point-bending configuration. A method for extracting the *J*-integral from a single displacement field is developed for this loading configuration under tensile load dominated conditions. The measurement of crack tip opening displacements are shown to vary linearly with the *J*-integral as in homogeneous counterparts thereby ascertaining the linkage between the crack tip behavior and a global parameter for an elasto-plastic interface. The plastic crack tip mode mixity is also evaluated from the measurements and plasticity is seen to greatly increase the mode mixity at the crack tip obtained from elastic analysis. The *J*-integral and crack growth measurements are used to develop crack growth resistance curve for the bimaterial and obtain critical value of J_C at crack initiation. The full-field optical measurements have revealed the possibility of using a simplified approach for developing crack growth resistance curves using a single-strain gage. This method seems attractive

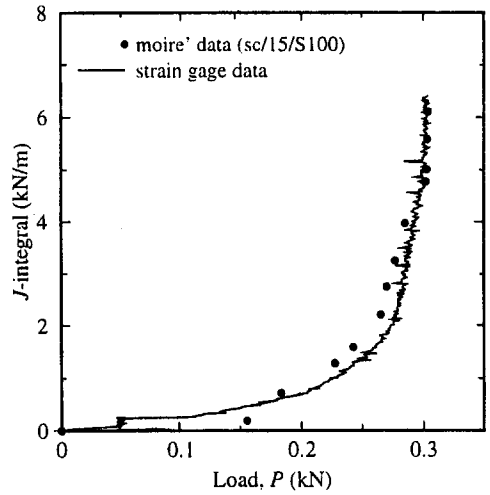

Fig. 13 Comparison of the *J*-integral estimated from optical and strain gage data

for large-scale fracture testing purposes using this geometry wherein a soft material is bonded to a stiff substrate. The method is successfully demonstrated. The value of J_C for the interface is in the range of 1.9–2.0 kN/m with a mode mixity of about 21 deg at crack initiation.

Acknowledgments

The support of the research by NSF grant CMS-9313153 is gratefully acknowledged. Partial support of the research from Alabama Microelectronics Science and Technology Center at Auburn University is also greatly appreciated. Authors would like to thank Mr. R. J. Butcher for providing computational assistance during this research.

References

Busso, E. P., Kitano, M., and Kumazawa, T., 1992, "A Visco-Plastic Constitutive Model for 60/40 Tin-Lead Solder Used in IC Package Joints," *Journal of Engineering Materials and Technology,* Vol. 114, pp. 331–337.

Enke, N. F., Killinski, T. J., Schroeder, L., and Lesniak, R., 1989, "Mechanical Behaviors of 60/40 Tin-Lead Solder Lap Joints," *IEEE Transactions on Components, Hybrids and Manufacturing Technology,* Vol. 12, No. 4, pp. 459–468.

Kang, B. S. J., and Kobayashi, A. S., 1988, "*J*-Estimation Procedure Based on Moiré Interferometry Data," *Journal of Pressure Vessel Technology,* Vol. 110, pp. 291–300.

Krishnamoorthy, H., and Tippur, H. V., 1998, "Extracting Fracture Parameters Using Local Collocation of Full-Field Displacement Data: A modified approach," *Experimental Techniques,* Vol. 22, No. 1, pp. 22–26.

Logsdon, W. A., Liaw, P. K., and Burke, M. A., 1990, "Fracture Behavior of 63Sn-37Pb solder," *Engineering Fracture Mechanics,* Vol. 36, No. 2, pp. 183–218.

O'Dowd, N. P., Shih, C. F., and Stout, M. G., 1992, "Test Geometries for Measuring Interfacial Fracture Toughness," *International Journal of Solids and Structures,* Vol. 29, No. 5, pp. 571–589.

Pratt, R. E., Stromswold, E. I., and Quesnel, D. J., 1994, "Mode-I Fracture Toughness Testing of Sn-Pb Solder Joints," *Journal of Electronic Materials,* Vol. 23, No. 4, pp. 375–381.

Read, D. T., 1981, "Experimental Method for Direct Evaluation of the *J*-Contour Integral," ASTM-STP 791, pp. 199–213.

Sharma, S. M., and Aravas, N., 1991, "Determination of Higher-Order Terms in Asymptotic Elasto-Plastic Crack Tip Solutions," *Journal of the Mechanics and Physics of Solids,* Vol. 39, pp. 1043–1072.

Shih, C. F., 1981, "Relationship Between the *J*-Integral and the Crack Opening Displacement for Stationary and Extending Cracks," *Journal of the Mechanics and Physics of Solids,* Vol. 29, No. 4, pp. 305–326.

Shih, C. F., Asaro, R. J., 1989, "Elastic-Plastic Analysis of Cracks on Bimaterial Interfaces: Part II—Structure of Small-Scale Yielding Fields," ASME *Journal of Applied Mechanics,* Vol. 56, pp. 763–779.

Shih, C. F., 1991, "Cracks on Bimaterial Interfaces: Elasticity and Plasticity Aspects," Materials Science and Engineering, Vol. A143, pp. 77–90.

Sinha, J. K., Tippur, H. V., and Xu, L., 1997, "An Interferometric and Finite Element Analysis of Interfacial Crack Tip Fields: Role of 3-D Stress Variations," *International Journal of Solids and Structures,* Vol. 34, No. 6, pp. 741–754.

Skipor, A. F., Harren, S. V., and Botsis, J., 1995, "The Effect of Mechanical Constraint on the Flow and Fracture of 63/37 Sn/Pb Eutectic Alloy," *Engineering Fracture Mechanics,* Vol. 52, No. 4, pp. 647–669.

Skipor, A. F., Harren, S. V., and Botsis, J., 1996, "On the Constitutive Response of Sn/Pb Solder," *Journal of Engineering Materials and Technology,* Vol. 118, pp. 1–11.

Yamada, S. E., 1989, "Fracture Mechanics Approach to Soldered Joint Cracking," *IEEE Transaction on Components Hybrids and Manufacturing Technology,* Vol. 12, No. 1, pp. 99–104.